AIAA JOURNAL
Vol. 43, No. 5, May 2005

Microstructural Effects in Multilayers with Large Moduli Contrast Loaded by Flat Punch

Linfeng Chen*
University of Virginia, Charlottesville, Virginia 22904
Edward E. Urquhart†
Märkisches Werk, D-58553 Halver, Germany
and
Marek-Jerzy Pindera‡
University of Virginia, Charlottesville, Virginia 22904

An efficient solution methodology is employed for the frictionless contact of half-planes built up with large number of layers to study the effect of microstructural refinement on the surface and subsurface stress fields. Half-planes with increasing numbers of alternating stiff and soft layer pairs spanning a fixed depth below the top surface are considered to determine the convergence behavior of the contact pressure and subsurface stresses relative to the corresponding quantities in fully or partially homogenized configurations with macroscopically equivalent properties. The results indicate that not all stress components converge to the corresponding values in the fully homogenized configuration with increasing microstructural refinement. This is only achieved by a partial homogenization wherein the layered half-plane is homogenized below a certain depth with the top surface layers retained. The number of retained surface layers required for an accurate stress field reproduction depends on the punch length and microstructural scale and depth of the alternating layers. The characteristic contact pressure profiles observed in the layered configurations suggest a basis for the development of a sensing technique for the microstructural architecture and property identification of the subsurface region.

Nomenclature

B_i	=	influence coefficients in the contact pressure representation
C_{ij}	=	elements of the stiffness matrix of an elastic material
E, G, ν	=	Young's and shear moduli and Poisson's ratio
$F_i(s), G_i(s)$	=	coefficients in the Fourier-transformed displacements
H	=	depth of the alternating hard and soft layers
h_h, h_s	=	thicknesses of hard and soft layers comprising layered half-planes
i	=	imaginary number $\sqrt{-1}$
$\boldsymbol{K}_{ij}^k$	=	submatrices of the local stiffness matrix of kth layer
p	=	pressure in the flat punch contact region
s	=	Fourier-transform parameter
$T_i(x)$	=	Chebychev polynomial of the first kind
$\bar{\boldsymbol{T}}_k^+, \bar{\boldsymbol{T}}_k^-$	=	top/bottom-surface Fourier-transformed traction vectors in kth layer
$\bar{\boldsymbol{U}}_k^+, \bar{\boldsymbol{U}}_k^-$	=	top/bottom-surface Fourier-transformed displacement vectors in kth layer
u, v, w	=	x, z coordinate-dependent displacement components
λ, μ	=	Lame's constants
$\sigma_{xx}, \sigma_{xz}, \sigma_{zz}$	=	x, z coordinate-dependent stress components

Received 15 June 2004; revision received 1 November 2004; accepted for publication 2 November 2004.

*Research Assistant, Civil Engineering Department.
†Managing Director, Halver Haus Heide 21.
‡Professor of Applied Mechanics, Civil Engineering Department.

Introduction

LAYERED media appear in a variety of engineering applications and problems. Examples range from geotechnical problems involving stratified media[1] and soil mechanics analysis[2] to stress analysis of modern laminated composites[3] and advanced material concepts such as functionally graded and multifunctional materials.[4] Recent advances in materials science and manufacturing extend the implementation of layered media concepts to piezoelectric,[5] microelectronic, and most recently nanotechnological applications. Many of these problems involve indentation by a probe of a known profile, such as conical or pyramidal in the case of three-dimensional problems and flat or parabolic in the case of plane problems. This class of problems is known as contact problems and has been studied extensively in the context of homogeneous and (to a lesser extent) multilayered half-spaces and finite depth configurations using both analytical and numerical techniques, compare Lane[6] and Seyidmamedov.[7] Analytical techniques are efficient in applications that can be modeled using plane or axisymmetric elasticity assumptions.

The plane elasticity contact problem of a rigid punch indenting an arbitrarily laminated multilayered half-plane (Fig. 1), can be solved conveniently using the local/global stiffness matrix formulation originally proposed by Bufler[8] in the context of isotropic layered media and subsequently extended to arbitrarily laminated composite half-planes by Pindera.[9] The local/global stiffness matrix formulation provides a systematic framework for treating layered media with an arbirary number of layers, leads to a substantial reduction in the global system of equations that must be solved, and facilitates extraction of the correct form of the governing integral equation for the pressure distribution underneath a flat or parabolic punch (or the crack opening displacement between adjacent layers in the case of crack problems). Recently, Ramirez and Heyliger[10] extended this formulation to layered half-spaces containing piezoelectric layers employed in the fabrication of so-called smart materials that are being developed for a wide range of applications, including the aircraft industry.

Analysis of elastic media containing very large numbers of layers involves some computational effort even when the local/global

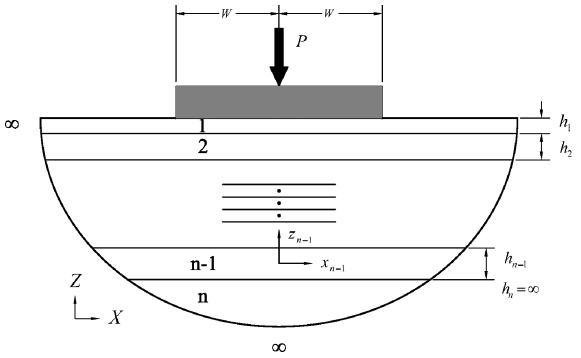

Fig. 1 Arbitrarily layered half-plane indented by a rigid flat punch.

stiffness matrix approach is employed. It is, therefore, natural to inquire whether the analysis can be simplified by replacing the actual microstructure or a part of it by equivalent properties obtained from a homogenization scheme without sacrificing the accuracy with which the local surface and subsurface stress fields are determined. For instance, homogenization of the actual microstructure is a standard practice in the analysis of functionally graded materials (Bansal and Pindera[11]). In the context of the multilayered media contact problem, two issues need to be addressed with respect to homogenization. The first is the effect of homogenization on the surface response dictated by the contact pressure distribution and contact area or indentation depth. The second issue is the effect of homogenization on the local character of the subsurface stress fields.

These issues are investigated herein in the contex of the flat punch contact on a periodically layered half-plane consisting of an alternating sequence of stiff and soft layers. The flat punch profile is employed as it produces large stress gradients at the corners in the presence of which the replacement of the actual layered microstructure by an equivalent homogenized medium may be questionable. Many schemes have been proposed to determine homogenized properties of heterogeneous materials/structures.[12] Here, we employ the method proposed by Postma[1] for wave propagation in a stratified medium that is applicable to periodic layered configurations consisting of homogeneous, isotropic layers.

In the next section, we present a brief summary of the local/global stiffness matrix approach for the solution of plane contact problems involving media with large numbers of layers under loading by a rigid and frictionless flat punch. Then, we investigate the convergence of the contact pressure and subsurface stresses as a function of microstructural refinement near the top surface to the corresponding quantities in the presence of either full or partial homogenization of the layered configuration. Our aim is to shed light on the conditions under which the homogenization scheme may be valid in the presence of large stress gradients and microstructural details in this class of contact problems. An interesting outcome of this investigation is the identification of characteristic contact pressure profiles that appear to depend uniquely on the architecture of the layered microstructure in the immediate vicinity of the top surface and the relative rigid punch width. These characteristic profiles can potentially provide a basis for the development of a sensing technique for microstructural architecture and property identification of the subsurface region.

Multilayer Frictionless Contact Problem

Determination of Contact Pressure

As shown by Pindera and Lane[13] and Urquhart and Pindera[14] for rigid circular and flat punches, the frictionless contact problem of multilayered half-planes reduces to the solution of a standard singular integral equation for the unknown contact pressure irrespective of the number of layers comprising the half-plane. This singular integral equation, characterized by a Cauchy-type kernel, whose solution can be obtained using the collocation technique developed by Erdogan[15] and Erdogan and Gupta,[16] can be readily derived from the global stiffness matrix of a layered structure in the Fourier-transform domain

$$\begin{bmatrix} \boldsymbol{K}_{11}^1 & \boldsymbol{K}_{12}^1 & \mathbf{0} & \cdot & \mathbf{0} \\ \boldsymbol{K}_{21}^1 & \left(\boldsymbol{K}_{22}^1 + \boldsymbol{K}_{11}^2\right) & \boldsymbol{K}_{12}^2 & \cdot & \mathbf{0} \\ \mathbf{0} & \boldsymbol{K}_{21}^2 & \left(\boldsymbol{K}_{22}^2 + \boldsymbol{K}_{11}^3\right) & \cdot & \mathbf{0} \\ \mathbf{0} & \mathbf{0} & \boldsymbol{K}_{21}^3 & \cdot & \mathbf{0} \\ \cdot & \cdot & \cdot & \cdot & \mathbf{0} \\ \mathbf{0} & \cdot & \cdot & \cdot & \left(\boldsymbol{K}_{22}^{n-1} + \boldsymbol{K}_{11}^{*n}\right) \end{bmatrix} \times \begin{bmatrix} \bar{\boldsymbol{U}}_1 \\ \bar{\boldsymbol{U}}_2 \\ \cdot \\ \cdot \\ \cdot \\ \bar{\boldsymbol{U}}_n \end{bmatrix} = \begin{bmatrix} \bar{\boldsymbol{T}}_1 \\ \mathbf{0} \\ \cdot \\ \cdot \\ \cdot \\ \mathbf{0} \end{bmatrix} \tag{1}$$

where $\bar{\boldsymbol{U}}_1 = [\bar{w}_1/i, \bar{u}_1, \bar{v}_1]^T$ and $\bar{\boldsymbol{T}}_1 = [\bar{p}/is, 0, 0]^T$ are the Fourier-transformed displacement and traction vectors on the top surface of the multilayered half-plane's very first layer, that is, $z_1 = +h_1/2$ (Fig. 1), $\bar{p}$ is the Fourier transform of the unknown normal stress $\bar{\sigma}_{zz}^1$ or pressure in the contact region $|x| \le w$,

$$\bar{\sigma}_{zz}^1\left(\frac{s, +h_1}{2}\right) = \bar{p}(s) = \frac{1}{\sqrt{2\pi}} \int_{-w}^{+w} p(t) e^{ist} \mathrm{d}t \tag{2}$$

and $\bar{\boldsymbol{U}}_i, i = 2, \ldots, n$, are the Fourier-transformed interfacial displacement vectors that ensure that the displacement components are continuous across the layer interfaces. The 3×3 submatrices $\boldsymbol{K}_{ij}^k$ are the elements of a local stiffness matrix for the kth layer that relates the Fourier-transformed displacement components $\bar{\boldsymbol{U}}_k^+ = [\bar{w}_k^+/i, \bar{u}_k^+, \bar{v}_k^+]^T$ and $\bar{\boldsymbol{U}}_k^- = [\bar{w}_k^-/i, \bar{u}_k^-, \bar{v}_k^-]^T$ at the top $(+)$ and bottom $(-)$ surface of the kth layer, that is, $z_k = \pm h_k/2$, to the corresponding traction components $\bar{\boldsymbol{T}}_k^+ = [\bar{\sigma}_{zz}^{k+}/is, \bar{\sigma}_{xz}^{k+}/s, \bar{\sigma}_{yz}^{k+}/s]^T$, and $\bar{\boldsymbol{T}}_k^- = [-\bar{\sigma}_{zz}^{k-}/is, -\bar{\sigma}_{xz}^{k-}/s, -\bar{\sigma}_{yz}^{k-}/s]^T$,

$$\begin{bmatrix} \boldsymbol{K}_{11}^k & \boldsymbol{K}_{12}^k \\ \boldsymbol{K}_{21}^k & \boldsymbol{K}_{22}^k \end{bmatrix} \begin{bmatrix} \bar{\boldsymbol{U}}_k^+ \\ \bar{\boldsymbol{U}}_k^- \end{bmatrix} = \begin{bmatrix} \bar{\boldsymbol{T}}_k^+ \\ \bar{\boldsymbol{T}}_k^- \end{bmatrix} \tag{3}$$

The elements of the four 3×3 submatrices $\boldsymbol{K}_{ij}^k$ have been derived explicitly in terms of a layer's material properties, thickness, and Fourier-transform parameter s by Pindera[9] for monoclinic, orthotropic, and (transversely) isotropic layers on solving Navier's equations for the displacement field $w(x, z)$, $u(x, z)$, $v(x, z)$ in the Fourier-transform domain. The global stiffness matrix is assembled in the form given in Eq. (1) by directly enforcing the displacement continuity at the interfaces separating adjacent layers on setting $\bar{\boldsymbol{U}}_k^-$ and $\bar{\boldsymbol{U}}_{k+1}^+$, $k = 2, \ldots, n$, to common values, $\bar{\boldsymbol{U}}_k^- = \bar{\boldsymbol{U}}_{k-1}^+ = \bar{\boldsymbol{U}}_k$, and summing up the traction vectors on either side of the interface to zero, $\boldsymbol{T}_k^- + \bar{\boldsymbol{T}}_{k+1}^+ = \mathbf{0}$.

The singular equation for the unknown pressure $p(x)$ in the contact region $|x| \le w$ is obtained by first inverting the global stiffness matrix to find the relationship between the transforms of the normal stress $\sigma_{zz}^1 = p(x)$ and the displacement $w_1(x)$ of the top layer directly underneath the punch,

$$\bar{w}_1(s) = H_{11}(s)\bar{p}(s)/s \tag{4}$$

where $H_{11}(s)$ is the (1, 1) element of the inverse of the global stiffness matrix. We note that $H_{11}(s)$ exhibits the following behavior as s approaches infinity:

$$\lim_{s \to \pm\infty} H_{11}(s) = \mathrm{sgn}(s) H_{11}^* \tag{5}$$

where H_{11}^* is a constant, which gives rise to a singular kernel in the integral equation governing the unknown contact pressure distribution. To extract the singular kernel, $H_{11}(s)$ is decomposed into singular and regular parts, $\mathrm{sgn}(s)\ H_{11}^*$ and $H_{11}^0(s) = H_{11}(s) - \mathrm{sgn}(s) H_{11}^*$,

respectively. Subsequently, when Eq. (4) is used in conjunction with the mixed boundary condition on the top surface of the layered half-plane, which requires that in the contact region the displacement and the punch profile slopes are compatible while outside the contact region the traction vector vanishes, an integral equation involving the unknown pressure over the contact region is obtained in the form

$$\frac{\mathrm{d}}{\mathrm{d}x}w_1(x) = \frac{-i}{\sqrt{2\pi}}\int_{-\infty}^{+\infty}\left[\mathrm{sgn}(s)H_{11}^{*} + H_{11}^{0}(s)\right]\bar{p}(s)e^{-isx}\,\mathrm{d}s \qquad |x| \le w \quad (6)$$

where the slope of the surface vertical displacement in the contact region is dictated by the punch profile. Equation (6) is reduced to one containing a Cauchy kernel on using the relation between the Fourier and finite Hilbert transforms of the contact pressure (see Gladwell[17]),

$$\frac{-i}{\sqrt{2\pi}}\int_{-\infty}^{+\infty}\mathrm{sgn}(s)\,\bar{p}(s)e^{-isx}\,\mathrm{d}s = \frac{1}{\pi}\int_{-w}^{+w}\frac{p(t)}{t-x}\,\mathrm{d}t \quad (7)$$

Finally, when the odd–even properties of the regular kernel $H_{11}^{0}(s)$ are used, integration limits for the regular integral may be changed and the following form of Eq. (6) is obtained:

$$\frac{\mathrm{d}}{\mathrm{d}x}w_1(x) = \frac{H_{11}^{*}}{\pi}\int_{-w}^{+w}\frac{p(t)}{t-x}\,\mathrm{d}t + \frac{1}{\pi}\int_{0}^{+\infty}\int_{-w}^{+w}H_{11}^{0}(s)p(t) \times \sin s(t-x)\,\mathrm{d}t\,\mathrm{d}s \qquad |x| \le w \quad (8)$$

A numerical collocation technique for solving singular integral equations of the form just given has been developed by Erdogan[15] and Erdogan and Gupta.[16] The contact pressure is represented by Chebychev polynomials of the first or second kind, depending on whether the punch is flat or circular, and orthogonality properties of these polynomials are used to reduce Eq. (8) to a linear system of algebraic equations representing the unknown contact pressure distribution at selected collocation points. In particular, for the flat punch the contact pressure $p(x)$ is approximated as

$$p(x) = \frac{F(x)}{\sqrt{1-x^2}}, \qquad F(x) = \sum_{i=0}^{n}B_iT_i(x)$$
$$T_i(x) = \cos(i\theta), \qquad \cos(\theta) = x \quad (9)$$

where $T_i(x)$ is a Chebychev polynomial of the first kind, $1/\sqrt{(1-x^2)}$ is the associated weight function, and the B_i are the unknown influence coefficients. Erdogan shows that Eq. (8) can be reduced to the following system of linear equations:

$$\sum_{k=1}^{n}\frac{1}{n}F(t_k)\left[\frac{1}{t_k-x_r}+\pi K_0(x_r,t_k)\right] = f(x_r) \qquad r = 1,\ldots,n-1 \quad (10)$$

where $t_k = \cos[(\pi/2n)(2k-1)]$, $x_r = \cos[\pi r/n]$, and, the inhomogeneous term is given by the slope of the punch, $f(x_r) = (\mathrm{d}/\mathrm{d}x)w_1(x_r)/H_{11}^{*}$, which is zero for a flat punch. The additional equation necessary for the solution of the unknown values of $F(t_k)$ in Eq. (10) at the $n-1$ collocation points t_k obtained from Eq. (9) comes from the load condition that states that the contact pressure must integrate to yield the total applied load,

$$\sum_{k=1}^{n}\frac{\pi}{n}F(t_k) = P = \text{load} \quad (11)$$

Finally, the system of Eqs. (10) and (11) can be further reduced by noting that the regular kernel $K_0(x_r, t_k)$ in Eq. (10)

$$K_0(x,t) = \frac{1}{\pi}\int_{0}^{+\infty}\frac{H_{11}^{0}(s)}{H_{11}^{*}}\sin s(t-x)\,\mathrm{d}s \quad (12)$$

is symmetric with respect to $r = n/2$ and is, therefore, evaluated only from $r = 1$ to $(n/2)$.

Determination of the Subsurface Stress Fields

Within a particular layer, the Fourier-transformed stress components in the x–z plane, $\bar{\sigma}_{zz}(s,z)$, $\bar{\sigma}_{xz}(s,z)$, and $\bar{\sigma}_{xx}(s,z)$, are given in terms of the corresponding displacement components $\bar{u}(s,z)$ and $\bar{w}(s,z)$ through Hooke's law,

$$\bar{\sigma}_{zz}(s,z) = -isC_{12}\bar{u}(s,z) + C_{11}\bar{w}_{,z}(s,z)$$
$$\bar{\sigma}_{xz}(s,z) = \tfrac{1}{2}(C_{11}-C_{12})[\bar{u}_{,z}(s,z) - is\bar{w}(s,z)]$$
$$\bar{\sigma}_{xx}(s,z) = -isC_{11}\bar{u}(s,z) + C_{12}\bar{w}_{,z}(s,z) \quad (13)$$

where the subscripted comma followed by the letter z denotes derivative with respect to z and C_{11} and C_{12} are the stiffness matrix elements of the isotropic layer. The Fourier-transformed displacement components, in turn, are given by

$$\bar{u}(s,z) = [F_1(s) + zF_2(s)]\cosh(sz) + [G_1(s) + zG_2(s)]\sinh(sz)$$
$$\bar{w}(s,z) = i[G_1(s) + (R/s)F_2(s) + zG_2(s)]\cosh(sz) + i[F_1(s) + (R/s)G_2(s) + zF_2(s)]\sinh(sz) \quad (14)$$

where $R = -(3C_{11}-C_{12})/(C_{11}+C_{12})$ and, the Fourier coefficients F_1, F_2, G_1, and G_2 for an isotropic layer can be expressed in terms of the interfacial displacements,

$$\begin{bmatrix}F_1(s)\\G_2(s)\end{bmatrix} = \begin{bmatrix}\cosh\left(\frac{sh}{2}\right) & \frac{h}{2}\sinh\left(\frac{sh}{2}\right)\\ \sinh\left(\frac{sh}{2}\right) & \frac{h}{2}\cosh\left(\frac{sh}{2}\right)+\frac{R}{s}\sinh\left(\frac{sh}{2}\right)\end{bmatrix}^{-1} \times \begin{bmatrix}\frac{\bar{u}^{+}+\bar{u}^{-}}{2}\\ \frac{\bar{w}^{+}-\bar{w}^{-}}{2i}\end{bmatrix}$$

$$\begin{bmatrix}F_2(s)\\G_1(s)\end{bmatrix} = \begin{bmatrix}\frac{h}{2}\cosh\left(\frac{sh}{2}\right) & \sinh\left(\frac{sh}{2}\right)\\ \frac{h}{2}\sinh\left(\frac{sh}{2}\right)+\frac{R}{s}\cosh\left(\frac{sh}{2}\right) & \cosh\left(\frac{sh}{2}\right)\end{bmatrix}^{-1} \times \begin{bmatrix}\frac{\bar{u}^{+}-\bar{u}^{-}}{2}\\ \frac{\bar{w}^{+}+\bar{w}^{-}}{2i}\end{bmatrix} \quad (15)$$

Once the contact pressure profile is known, the contact problem is reduced to a boundary-value problem of the first kind. The system of equations given by the global stiffness matrix relating the interfacial displacements to the now known external tractions (with the pressure distribution being the only nonzero traction component) is solved to obtain the interfacial displacements in the transform domain. The knowledge of the Fourier-transformed interfacial displacement components for a given layer allows the calculation of the Fourier-transformed displacement components at any vertical location in the layer using Eqs. (14) and (15) and, thus, the inplane stress components, Eq. (13). Application of the inverse Fourier transform to these equations through a very accurate numerical integration procedure described by Urquhart[18] produces the in-plane stresses in the x–z plane.

Numerical Results

The investigated layered half-plane is shown in Fig. 2. It consists of a sequence of alternating isotropic hard and soft layers of thickness h_h and h_s, respectively, attached to a transversely isotropic half-plane and is subjected to indentation by rigid flat indenters of variable width $2w$. Table 1 gives the elastic constants of the layers, with Young's moduli representative of glass or aluminum and

epoxy. The hard layers are three times thicker than the soft layers, that is, $h_h/h_s = 3$, the overall thickness or depth H of the alternating layers is fixed, and the punch width $2w$ is varied to produce the three ratios $2w/H = 0.5$, 2 and 4. The elastic properties of the supporting transversely isotropic half-plane with the x–y plane of isotropy given in Table 2 were generated by applying the Postma[1] homogenization scheme to an alternating sequence of hard and soft layers with the same material and geometric parameters as those of the

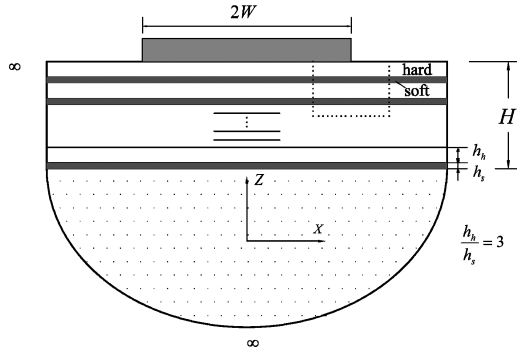

Fig. 2 Investigated geometry of layered half-plane consisting of alternating sequence of stiff and soft layers.

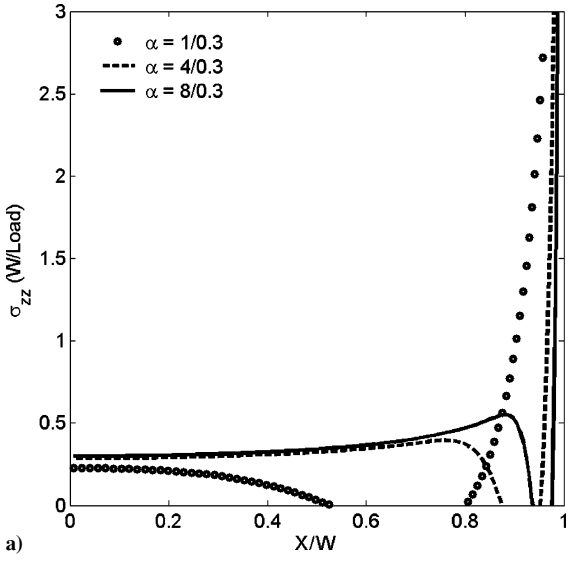

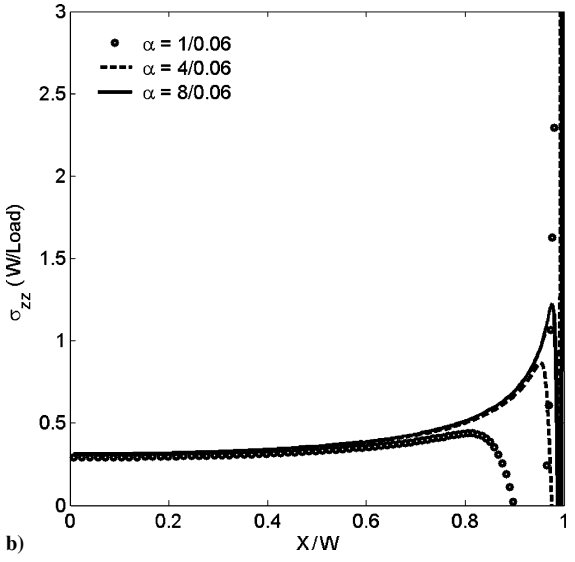

Fig. 3 Contact pressures for single hard layer bonded to a soft half-plane with Young's moduli ratio $\beta = 20$ for two sets of α ratios characteristic of hard-layer thickness employed in a) 20-layer configuration and b) 100-layer configuration.

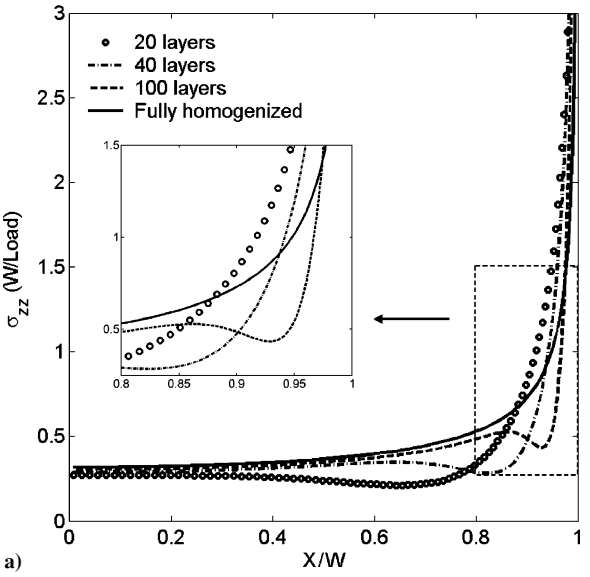

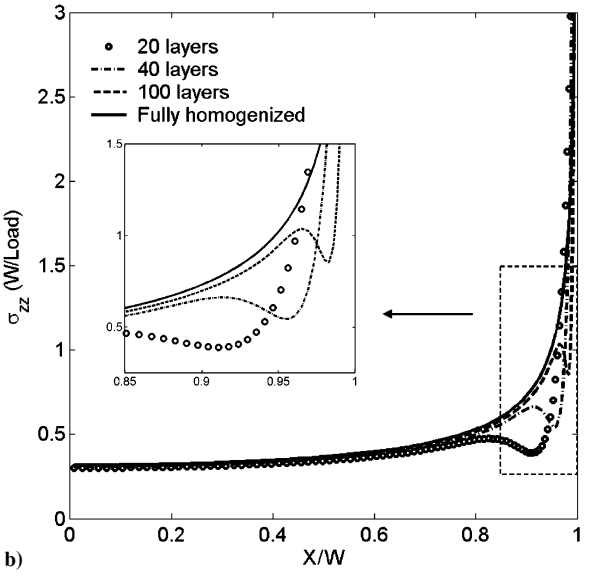

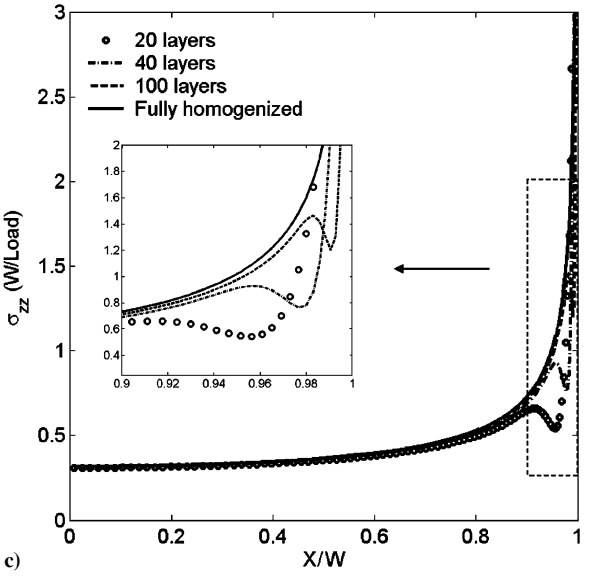

Fig. 4 Contact pressures for discretely layered configurations and equivalent homogenized half-plane: a) $2w/H = 0.5$, b) $2w/H = 2$, and c) $2w/H = 4$.

layers above the half-plane. The Postma model employs the moduli and thicknesses of discrete isotropic layers to determine the overall transversely isotropic properties of a periodically layered plane (see the Appendix), with the direction of anisotropy orthogonal to the plane of alternating layers. The homogenized properties depend only on the layer thickness ratio and not on the actual layer dimensions.

In the next section, the number of alternating layers is progressively increased within the fixed total thickness H from 20 to 100, keeping the overall volume fraction of the individual constituents constant, that is, fixed h_h/h_s ratio. The contact response and subsurface stress fields are compared to the corresponding quantities obtained when the discrete layers are replaced by a single homogeneous material with effective elastic properties obtained from the Postma model. In this case, the entire layered configuration becomes a single homogeneous half-plane with one set of transversely isotropic properties for which the contact pressure is readily obtained in closed form. As the number of layers is increased, producing an increasingly finer microstructure within the region spanning the depth H, the response of the layered half-plane is typically expected to approach the response of the homogenized Postma configuration, likely in a manner that depends on the punch width.

Table 1 Elastic properties of hard and soft layers within layered half-planes

Material	E, Msi	G, Msi	ν
Soft (epoxy)	0.50	0.185	0.35
Hard (aluminum)	10.0	3.759	0.33

Table 2 Homogenized elastic properties of periodically layered half-planes, with x–y or 1–2 plane of isotropy, based on the Postma model[a]

Property	Value
E_{11}, Msi	7.625
E_{33}, Msi	2.458
G_{12}, Msi	2.866
G_{13}, Msi	0.645
ν_{12}	0.330
ν_{13}	0.337

[a] $E_{11} = E_{22}$, etc.

To set the present results in perspective, we recall the response of a single stiff layer bonded to a much softer half-plane under the same loading. As shown by Shield and Bogy[19] for isotropic layers and by Urquhart and Pindera[14] for anisotropic composite layers, the local bending response of the stiff surface layer gives rise to separation within the contact region for certain geometric and material property ratios $\alpha = w/h_{\text{layer}}$ and $\beta = E_{\text{layer}}/E_{\text{plane}}$. Two-region contact involves separation of the punch from the surface layer in the middle of the contact region, whereas three-region contact is characterized by separation on either side of the punch's central region. Three-region contact pressure distribution is characterized by a nonzero magnitude in the central region, which decreases or dips down to zero as the symmetric separation regions are approached, remains zero within the separation regions, and then increases from zero to infinity as the right or left punch corner is approached. The zones corresponding to full, two-region, and three-region contact in the $1/\alpha - \beta$ space have been identified by Shield and Bogy[19] and replicated by Urquhart and Pindera[14] using the present analysis approach. Characteristic dips in the contact pressure are observed for those α, β combinations in the full contact region that approach three-region contact boundary along fixed α_0 or β_0 directions.

For the employed layer Young's moduli and punch and layer dimensions, all α, β ratios that characterize the response of a single stiff layer bonded to a much softer half-plane loaded by flat punch produce three-region contact. Figure 3 presents the normalized contact pressure distributions for this simple configuration with $\beta = 20$ and two sets of $\alpha = w/h_{\text{layer}}$ ratios that are characteristic of the hard-layer thickness in the 20-layer and 100-layer configurations

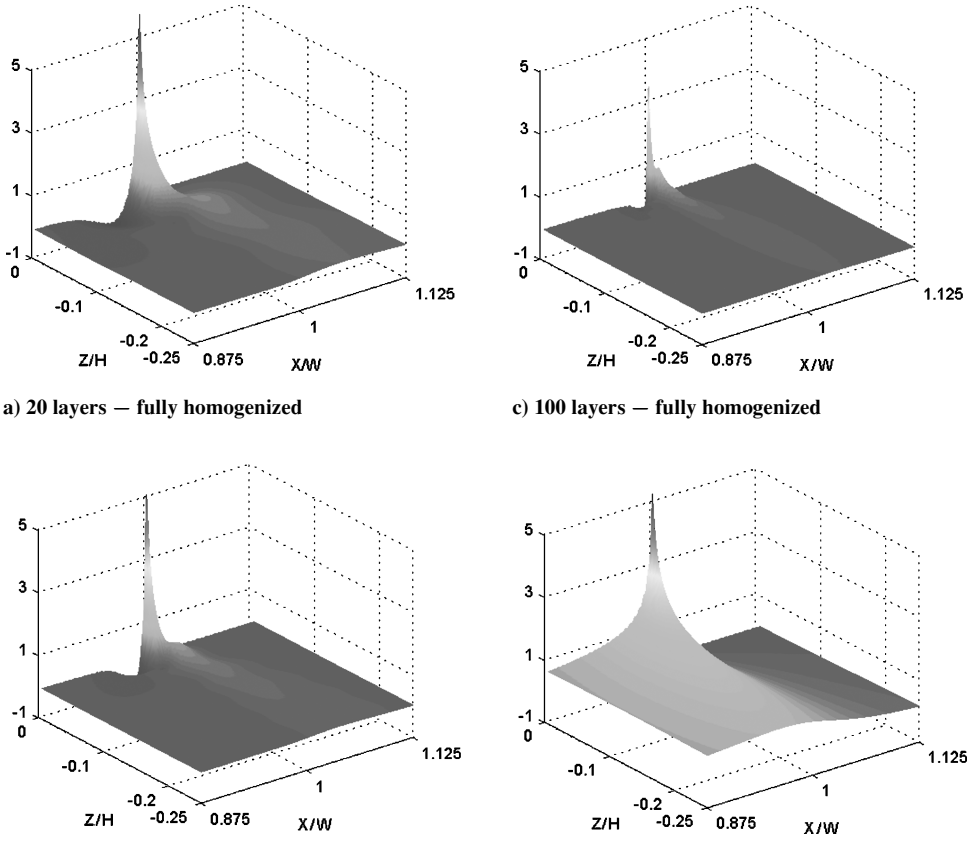

a) 20 layers — fully homogenized

c) 100 layers — fully homogenized

b) 40 layers — fully homogenized

d) Fully homogenized

Fig. 5 Differential σ_{zz} stress distributions within 20-, 40-, and 100-layer configurations relative to homogenized half-plane distribution for $2w/H = 4$, normalized by P/w.

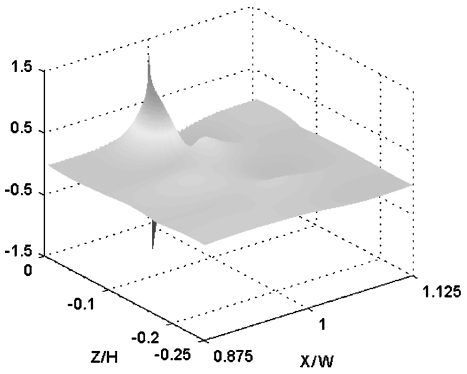

a) 20 layers — fully homogenized

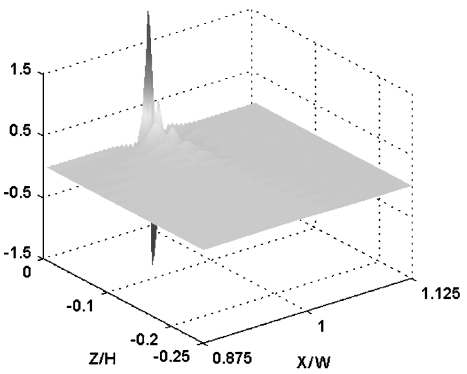

c) 100 layers — fully homogenized

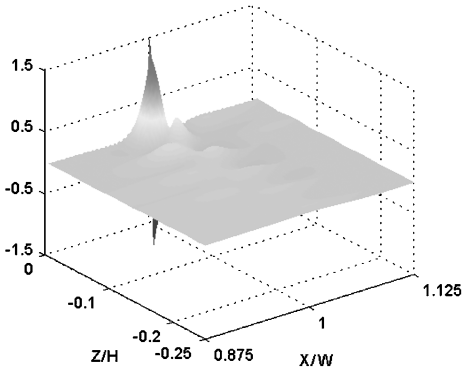

b) 40 layers — fully homogenized

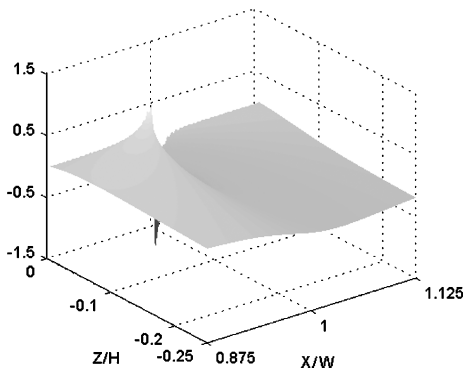

d) Fully homogenized

Fig. 6 Differential σ_{xz} stress distributions within 20-, 40-, and 100-layer configurations relative to homogenized half-plane distribution for $2w/H = 4$, normalized by P/w.

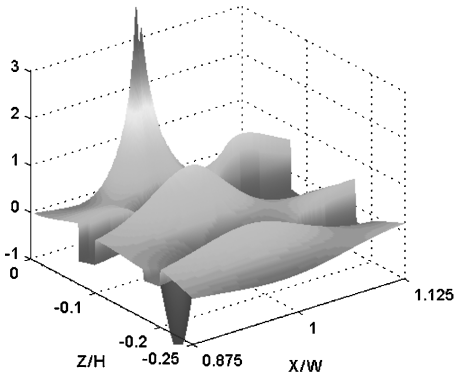

a) 20 layers — fully homogenized

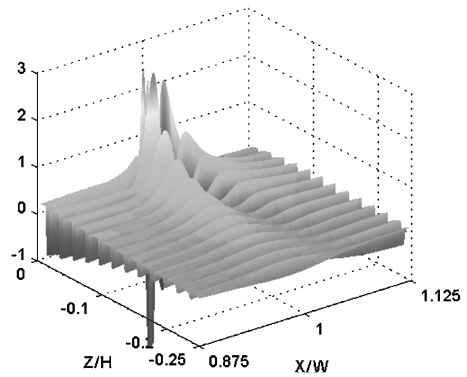

c) 100 layers — fully homogenized

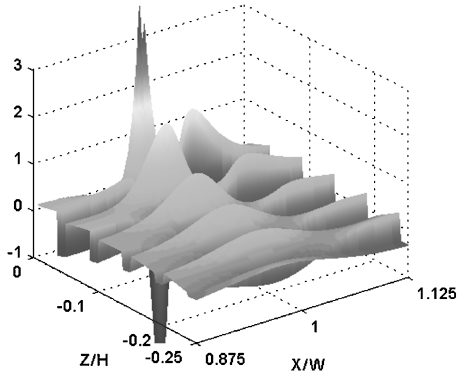

b) 40 layers — fully homogenized

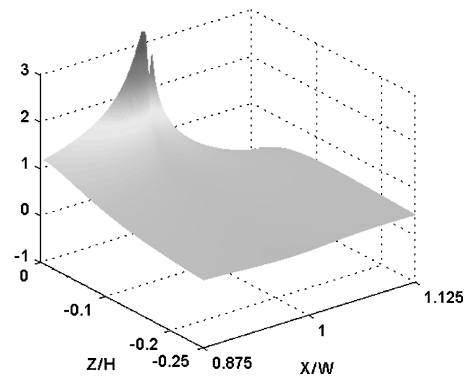

d) Fully homogenized

Fig. 7 Differential σ_{xx} stress distributions within 20-, 40-, and 100-layer configurations relative to homogenized half-plane distribution for $2w/H = 4$, normalized by P/w.

discussed in the next section. The profiles are normalized by the ratio of the applied load divided by the half-punch width. For each set of α ratios, the punch half-width was the same as that employed in the analysis of the layered configurations. As can be clearly seen, separation occurs for all α ratios at this particular value of β. Furthermore, for each set of α ratios, the separation region moves out toward the outer contact region with increasing α, whereas the interior pressure distributions exhibit more commonality over a greater region.

Discrete vs Fully Homogenized Configurations

Figure 4 shows the normalized contact pressure profiles for half-planes consisting of 20, 40, and 100 layers of alternating hard and soft plies within the region spanning the depth H for the three $2w/H$ ratios. These results were generated using a total of 96 collocation points in Eq. (10) for half-punch width on taking advantage of the contact pressure symmetry. Included in Fig. 4 for the different $2w/H$ ratios is the contact pressure distribution obtained for the homogeneous half-plane with Postma-homogenized equivalent moduli based on the same sequence of alternating hard and soft layers as in the layered configurations. These Postma pressure profiles are smooth and exhibit the well-known singular $1/\sqrt{[1-(x/w)^2]}$ behavior characteristic of fully homogeneous transversely isotropic or orthotropic half-planes. In contrast, the pressure profiles for the discrete-layer configurations exhibit departures from those of the homogenized configurations that are characterized by downward dips, similar to those seen in the single-layer cases in Fig. 3, in the interior before singular behavior is recovered at the punch corner. In none of the cases, however, are the dips of sufficient magnitude to cause separation. The extent of the deviations, including the magnitude and location of the dips, depends on the $2w/H$ ratio as in the single-layer cases, as well as on the number of plies in the layered configuration or the microstructural scale. For each $2w/H$ ratio, the contact pressure distributions for the discrete layer configurations tend to converge to the contact pressure distribution of the fully homogenized configuration with increasing number of alternating layers in the interior of the contact region. This is accompanied by a shift of the dips toward the punch exterior closer to the corner, localization of the dip profile, and an upward shift in the dip's local minimum.

Specifically, in the case of the smallest $2w/H$ ratio 0.5 (Fig. 4a), a noticeable difference in the pressure profiles of the Postma model and the 20-layer configuration is observed in the contact region $x/w > 0.4$, with the latter characterized by a gradual dip whose minimum occurs close to $x/w = 0.7$, whereas for the 100-layer configuration the difference is only significant in the region between $x/w = 0.85$ and $x/w = 0.95$ where the dip occurs. These differences decrease with increasing $2w/H$ ratio (Figs. 4b and 4c). In the $2w/H = 2$ case, the contact pressures of the discrete configurations are virtually the same as that of the homogenized half-plane up to around $x/w = 0.8$, at which point the 20-layer configuration pressure distribution begins to dip down. This distance increases with the increasing number of layers. In the $2w/H = 4$ case, the point of contact pressure deviation moves out to $x/w = 0.9$. However, the magnitude of the dips does not appear to decrease with microstructural refinement or increasing $2w/H$ ratio for our configurations.

The results shown in Fig. 3 for a single stiff layer bonded to a much softer homogeneous half-plane suggest that the downward dips observed in the contact pressure distributions of the layered configurations are rooted in the local bending of the surface layer(s) underneath the indenter. The underlying microstructural details mitigate the separation phenomenon by providing stiffer support for the surface layer(s), thereby raising the elevations of the dips' minima. This is similar to increasing the stiffness of the underlying half-plane in the case of a single layer bonded to a softer half-plane. Unlike the single-layer case, however, microstructural refinement plays a significant role in localizing the surface-layer bending effect by shifting the dip minima locations outward and upward. Smilar stress reversal behavior has been observed by Erdogan[20] along the interface of a layered coating with graded elastic moduli and a homogeneous substrate at the free edge under spatially uniform thermal loading. In this case, the microstructural coating refinement affected both the

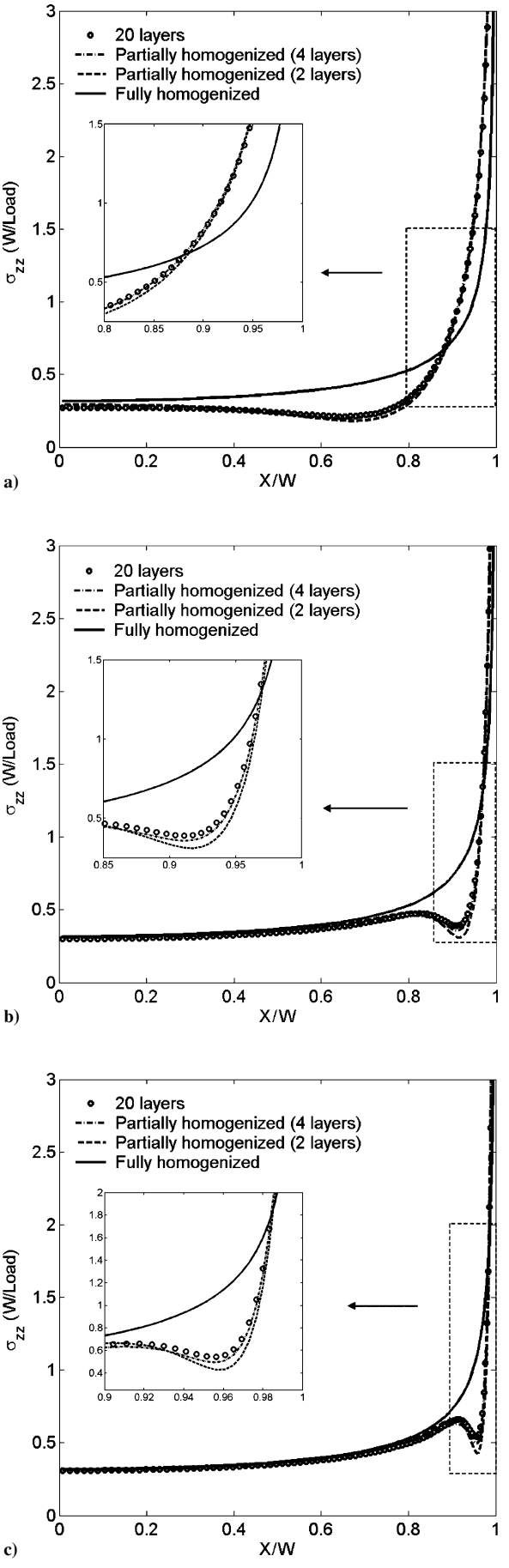

Fig. 8 Comparison of contact pressures in partially and fully homogenized configurations with that of discrete 20-layer configuration: a) $2w/H = 0.5$, b) $2w/H = 2$, and c) $2w/H = 4$.

character of the local stress reversal dip and the order of the free-edge stress singularity. The latter effect was due to the piecewise uniform manner of grading the layered coating's elastic moduli.

In summary, the contact pressure distribution in the Postma-based homogenized configuration becomes a better approximation of the contact pressure in a discrete-layer configuration with increasing $2w/H$ ratio and increasing microstructural refinement. In the $2w/H = 2$ case shown in Fig. 4b, the profiles for the 100-layer configuration and the Postma model are almost identical, with the exception of a small deviation near the outer edge of the contact region. In the $2w/H = 4$ case (Fig. 4c), the profiles for the 40-layer configuration and the Postma model are nearly identical through about 95% of the contact region, and the correlation is even better for the 100-layer structure. Nevertheless, the dips that move out toward the punch corners still persist even in the case of very fine microstructural details relative to the punch dimensions and appear to be caused by very localized bending of the surface layer bonded to the much softer layer beneath it even as the layers' thicknesses decrease with microstructural refinement. This places restrictions on the applicability of homogenization schemes in applications such as that considered herein.

To determine how far into the layered half-plane the microstructural effects propagate, subsurface σ_{zz}, σ_{xz}, and σ_{xx} stress distributions are compared to the corresponding distributions within the homogenized half-plane near the right punch corner in Figs. 5, 6, and 7, respectively. This comparison was carried out by subtracting the stress distributions within the single, fully homogenized half-plane from the distributions in the three-layered configurations to produce differential stress distributions at normalized $(x_i/w, z_i/H)$ locations in the region $0.875 \le x/w \le 1.125$, $-0.005 \ge z/H \ge -0.25$. These differential distributions were then normalized by the P/w ratio as was done for the contact pressure profiles. The number of points along the x and z axes used in this region for plotting the distributions was 206 and 137, respectively, with denser grid density close to the corner. The top surface was not included to exclude the singular stress components for presentation clarity. The selected region comprises 5, 10, and 25 layers within the 20-, 40-, and 100-layer configurations, respectively. The largest $2w/H$ ratio was used

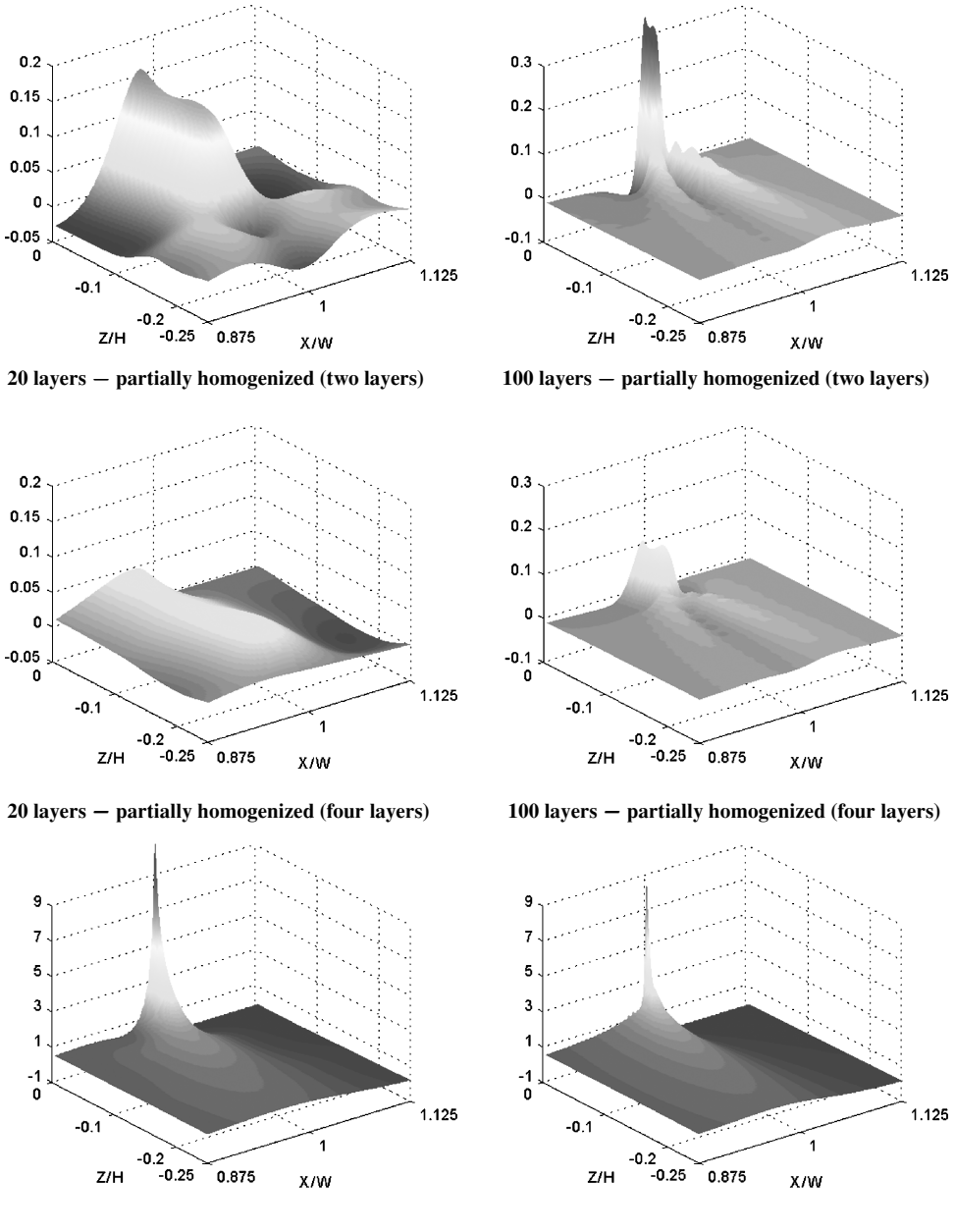

Fig. 9 Differential σ_{zz} stress distributions within partially homogenized 20- and 100-layer configurations relative to corresponding fully discrete configurations for $2w/H = 4$.

for this comparison for which the contact pressure distributions of the layered configurations differ from the homogenized case only in the immediate vicinity of the punch corners. Figures 5d, 6d, and 7d show the particular stress distribution within the single homogenized half-plane and provided as a reference.

The actual σ_{zz} stress distributions within the layered configurations (not shown) are continuous across the layer interfaces and smoothly approach the distribution within the fully homogenized half-plane outside of a small boundary layer near the punch corners, as can be deduced from the three differential distributions shown in Fig. 5. In the immediate vicinity of the punch corner, the region just below the top surface, within which the differential σ_{zz} stress tends to very high values, decreases with increasing microstructural refinement. However, the actual σ_{zz} stress component does not fully converge to the homogenized case even for the 100-layer configuration, where significant magnitudes of the differential stress persist in the decreasingly small boundary-layer region.

The σ_{xz} stress distributions, even though they are also continuous across the layer interfaces in the layered configurations, exhibit a somewhat different behavior relative to the homogenized distribution. First, the local maximum and minimum values that occur just below the top surface on either side of the vertical plane passing through the punch corner do not tend to converge to the corresponding values of the homogenized half-plane with increasing microstructural refinement, as seen in Fig. 6. In fact, the absolute values increase with increasing layer number. Thus, the actual microstructure of a layered configuration must be taken into account in cases where failure is initiated by the shear stress. Furthermore, the actual locations where these values occur, which are the same for the layered configurations, differ somewhat from the corresponding locations within the homogenized half-plane. Away from the locations where maximum and minimum σ_{xz} values occur, the shear stress distributions within the layered configurations converge to that of the homogenized half-plane in a nonmonotonic manner, characterized by fluctuations whose wavelength corresponds to the microstructural scale, in contrast with the σ_{zz} stress distributions.

Substantially greater fluctuations are observed in the σ_{xx} distributions within the layered configurations as suggested by the differential distributions in Fig. 7. These fluctuations are expected inasmuch as the layer interfaces are traversed because σ_{xx} is not a traction

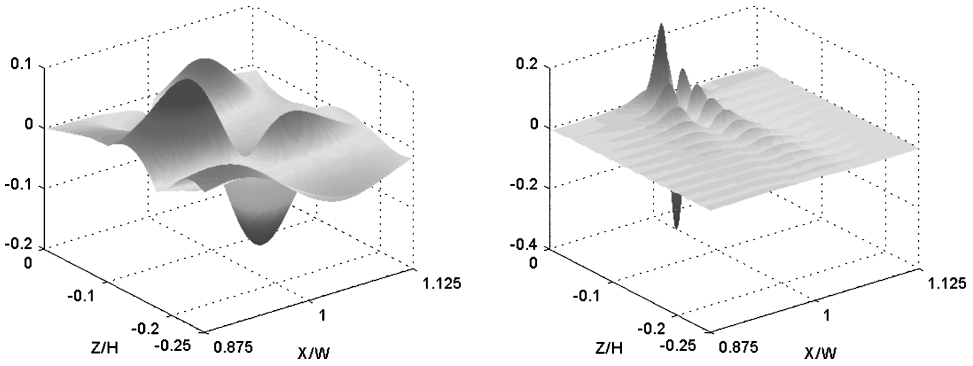

20 layers — partially homogenized (two layers) **100 layers — partially homogenized (two layers)**

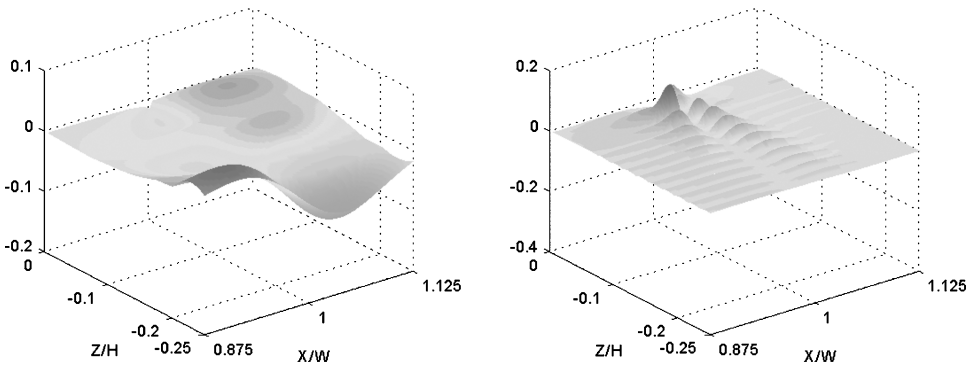

20 layers — partially homogenized (four layers) **100 layers — partially homogenized (four layers)**

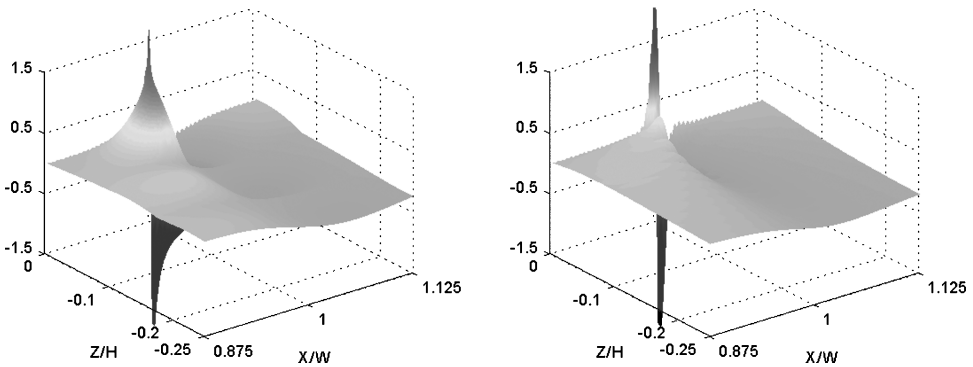

20 layers **100 layers**

Fig. 10 Differential σ_{xz} stress distributions within partially homogenized 20- and 100-layer configurations relative to corresponding fully discrete configurations for $2w/H = 4$.

component along the vertical direction and, thus, is not required to be continuous across layer interfaces, in contrast to the σ_{zz} and σ_{xz} distributions. The magnitude of the fluctuations reflects the Young's modulus mismatch between adjacent stiff and soft layers. These fluctuations do not occur in the fully homogenized half-plane, which explains the sign change in the differential σ_{xx} distributions absent in the actual distributions. Unlike the σ_{xz} distributions, the local maximum and minimum values of the σ_{xx} stress fields in the immediately vicinity of the punch corner do tend to those of the homogenized configuration with increasing microstructural refinement, albeit at a very slow rate as observed in the differential distributions.

Discrete vs Partially Homogenized Configurations

The differences in the contact pressure profiles and subsurface stress distributions between the layered and homogenized configurations shown earlier as a function of microstructural refinement suggest that full homogenization will never exactly duplicate the response of a layered configuration in the regions of high stress gradients. In particular, microstructural refinement appears to affect different stress components in a different manner vis-a-vis convergence to the homogenized configuration results. However, if just a few surface layers are retained, and the remaining microstructure replaced by an equivalent homogenized material, a closer approximation may be obtained. We call this partial homogenization. The few top surface layers allow the microstructure directly below the indenter to respond in nearly the same manner as in the fully discretized configuration, whereas the greatly reduced number of layers enhances considerably the computational efficiency.

To demonstrate this, the contact response of the 20-layer configuration is compared with the fully homogenized Postma model and partially homogenized structures with two and four surface layers retained for the three $2w/H$ ratios. Figure 8a shows the contact pressure profiles for the lowest $2w/H$ ratio, where it is observed that retaining just the top two surface layers and homogenizing the rest of the layered configuration is sufficient to duplicate the contact response almost identically throughout the entire contact region. Increasing the number of top surface layers to four eliminates the remaining slight differences. As already demonstrated, the contact

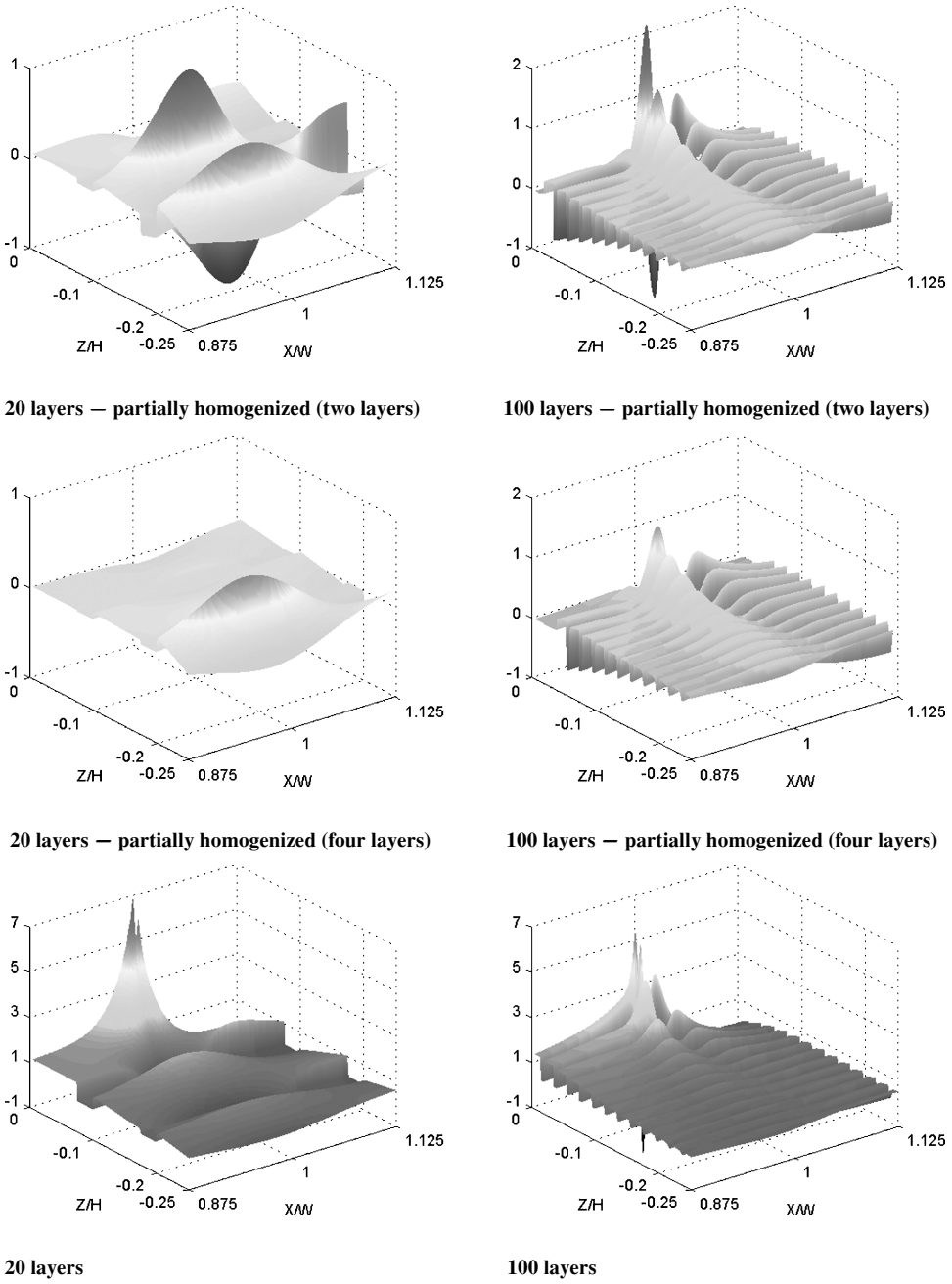

Fig. 11 Differential σ_{xx} stress distributions within partially homogenized 20- and 100-layer configurations relative to corresponding fully discrete configurations for $2w/H = 4$.

pressure profile of the fully homogenized half-plane deviates substantially from the 20-layer configuration profile.

As the width of the punch is increased, the number of layers needed to duplicate the response of the fully discretized structure increases because the thickness of the layers relative to the punch width decreases and the dips become more pronounced. Figures 8b and 8c show the contact pressure profiles for the intermediate and largest $2w/H$ ratios, respectively, where both two and four of the surface layers are retained. For the intermediate $2w/H$ ratio, the contact pressure profile for the case where two of the surface layers are retained does exhibit the characteristic dip seen in the fully discretized structure; however, the extent of the dip is visibly overestimated. The case where four layers are retained produces a much closer profile in the dip region. The trends are the same for largest $2w/H$ ratio; however, a somewhat greater number of layers need to be retained to model more accurately the response of the fully discretized configuration. The contact pressure profile of the fully homogenized half-plane demonstrates again the homogenization-based approach's inability to reproduce the local contact pressure details generated by the microstructural effects.

In Figs. 9–11, we present the normalized subsurface σ_{zz}, σ_{xz}, and σ_{xx} distributions within the corner region of the partially homogenized 20-layer and 100-layer configurations for the largest $2w/H$ ratio. The results from both the two and four surface layer configurations are shown for each configuration set. As before, normalized differential stress distributions are plotted that were generated by subtracting the stress distributions in the two sets of partially homogenized configurations from those of the fully discretized configurations. The actual normalized stress distributions of the fully discretized 20-layer and 100-layer configurations are included in Figs. 9–11 for reference.

The normalized differential σ_{zz} distributions shown in Fig. 9 indicate that the convergence of subsurface σ_{zz} stress fields in the partially homogenized configurations to the stress fields in the fully discretized configurations decreases with microstructural refinement. That is, it is slower for the 100-layer configuration than the 20-layer configuration. Furthermore, substantial reduction in the differential distributions is observed as the number of surface layers increases from two to four where the differences are quite small in both the 20-layer and 100-layer configurations. Similar observations hold for the normalized differential σ_{xz} stress distributions shown in Fig. 10. Alternatively, the normalized differential σ_{xx} stress distributions shown in Fig. 11 indicate that substantially more surface layers need to be retained to reduce the stress distribution differences between partially homogenized and fully discretized configurations to an extent comparable to that observed in the σ_{zz} and σ_{xz} stress distributions.

Conclusions

Comparison of stress distributions in discretely layered and homogeneous half-planes with equivalent homogenized properties indicates that, in the presence of high-stress gradients caused by the rigid punch corners, the surface and subsurface stress distribution differences persist with increasing microstructural refinement near the top surface. This holds even when very finely layered microstructures are employed and affects different stress components in different ways. Furthermore, the characteristic features of contact pressure distributions observed in layered configurations change in a predictable manner with both the microstructural refinement and the ratio of the punch width to the depth of the layered microstructure. As a practical consequence of technological importance, this suggests the possibility of contact test method development for interrogating the microstructural details and integrity of layered configurations using stiff pressure-sensitive materials or devices.

The results generated herein also provide evidence that the commonly employed and accepted homogenization techniques for periodic microstructures should be used with caution when dealing with stress analysis problems involving high-stress gradients. In particular, the boundary-layer effects that propagate into layered periodic microstructures in the presence of stress gradients can be significant and may not quickly converge even in an average sense to the homogenization-based results in the regions of high-stress gradients. We note that these results are also relevant to the analysis of functionally graded materials, where it is a common practice to replace an actual spatially variable microstructure produced by a distribution of phases with large property contrast with equivalent homogenized properties, thereby facilitating the application of standard elasticity solution techniques.

Finally, retaining the actual microstructural details in the regions of high-stress gradients while homogenizing the remaining microstructure is an effective technique to generate accurate results efficiently (by reducing the size of the mixed boundary-value problem that needs to be solved). In the context of flat contact problems on periodic layered media, the extent of homogenization depends on both the microstructural scale and the punch width and depth of the layered microstructure. The developed computational capability outlined herein provides a useful tool in generating guidance for such partial homogenization.

Appendix: Postma Model

The homogenized elastic stiffness matrix elements C_{ij} of the alternating layered medium are explicitly given in terms of the Lame's constants λ_i and μ_i of the individual isotropic layers $i = 1, 2$ and their thicknesses h_i in the form[1]

$$C_{11} = (1/D)\Big\{(h_1+h_2)^2(\lambda_1+2\mu_1)(\lambda_2+2\mu_2) + 4h_1h_2(\mu_1-\mu_2)[(\lambda_1+\mu_1)-(\lambda_2+\mu_2)]\Big\}$$

$$C_{12} = (1/D)\Big[(h_1+h_2)^2\lambda_1\lambda_2 + 2(\lambda_1h_1+\lambda_2h_2)(\mu_2h_1+\mu_1h_2)\Big]$$

$$C_{13} = (1/D)\{(h_1+h_2)[\lambda_1h_1(\lambda_2+2\mu_2)+\lambda_2h_2(\lambda_1+2\mu_1)]\}$$

$$C_{33} = (1/D)\Big[(h_1+h_2)^2(\lambda_1+2\mu_1)(\lambda_2+2\mu_2)\Big]$$

$$C_{44} = (h_1+h_2)\mu_1\mu_2/(h_1\mu_2+h_2\mu_1)$$

$$C_{66} = (\mu_1h_1+\mu_2h_2)/(h_1+h_2)$$

where $D = (h_1+h_2)[h_1(\lambda_2+2\mu_2)+h_2(\lambda_1+2\mu_1)]$ and $C_{11} = C_{22}$, $C_{44} = C_{55}$, and $C_{66} = (C_{11}-C_{12})/2$. These relations among the stiffness matrix elements indicate that the laminated medium is transversely isotropic with the x–y (or 1–2) plane of isotropy. The knowledge of the elastic stiffness matrix elements C_{ij} allows one to calculate the homogenized engineering constants shown in Table 2 using standard formulas, that is, $E_{11} = 1/S_{11}$, etc., where the compliance matrix elements S_{ij} are obtained from the inverse of the elastic stiffness matrix $\boldsymbol{C}$ or $\boldsymbol{C}^{-1} = \boldsymbol{S}$.

Acknowledgments

This research was supported by the NASA John H. Glenn Research Center at Lewis Field-through NASA Grant NAG3-2524 and the Ohio Aerospace Institute subcontract to the University of Virginia in support of NASA Contract NCC-878.

References

[1]Postma, G. W., "Wave Propogation in a Stratified Medium," *Journal of Geophysics*, Vol. 20, No. 4, 1955, pp. 780–806.

[2]Rowe, R. K., and Booker, J. R., "Finite Layer Analysis of Nonhomogeneous Soils," *Journal of Engineering Mechanics*, Vol. 108, No. 1, 1982, pp. 115–132.

[3]Pagano, N. J., "Exact Solutions for Rectangular Bidirectional Composites and Sandwich Plates," *Journal of Composite Materials*, Vol. 4, Jan. 1970, pp. 20–35.

[4]Paulino, G. H. (ed.) "Fracture of Functionally Graded Materials," *Engineering Fracture Mechanics*, Vol. 69, No. 14-16, 2002, pp. 1519–1812.

[5]Heyliger, P., "Static Behavior of Laminated Elastic Piezoelectric Plates," *AIAA Journal*, Vol. 32, No. 12, 1994, pp. 2481–2484.

[6]Lane, M. S., "The Frictionless Contact Problem of Anisotropic Multilayered Media," Ph.D. Dissertation, Civil Engineering Dept., Univ. of Virginia, Charlottesville, VA, Jan. 1991.

[7]Seyidmamedov, Z., "Finite-element Analysis of Frictionless Contact Problem for a Laminated Medium," *Mathematics and Computers in Simulation*, Vol. 58, No. 2, 2002, pp. 111–123.

[8]Bufler, H., "Theory of Elasticity of a Multilayered Medium," *Journal of Elasticity*, Vol. 1, No. 2, 1971, pp. 125–143.

[9]Pindera, M.-J., "Local/Global Stiffness Matrix Formulation for Composite Materials and Structures," *Composites Engineering*, Vol. 1, No. 2, 1991, pp. 69–83.

[10]Ramirez, G., and Heyliger, P., "Frictionless Contact in a Layered Piezoelectric Half-Space," *Smart Materials and Structures*, Vol. 12, No. 4, 2003, pp. 612–625.

[11]Bansal, Y., and Pindera, M.-J., "Efficient Reformulation of the Thermoelastic Higher-Order Theory for FGMs," *Journal of Thermal Stresses*, Vol. 26, No. 11-12, 2003, pp. 1055–1092.

[12]Kalamkarov, A. L., and Kolpakov, A. G., *Analysis, Design and Optimization of Composite Structures*, Wiley, New York, 1997.

[13]Pindera, M.-J., and Lane, M. S., "Frictionless Contact of Layered Half Planes: Part I—Analysis," *Journal of Applied Mechanics*, Vol. 60, No. 3, 1993, pp. 633–639.

[14]Urquhart, E. E., and Pindera, M.-J., "Incipient Separation Between a Frictionless Flat Punch and an Anisotropic Multilayered Half Plane," *International Journal of Solids and Structures*, Vol. 31, No. 18, 1994, pp. 2445–2461.

[15]Erdogan, F., "Approximate Solutions of Systems of Singular Integral Equations," *Journal of Applied Mathematics*, Vol. 17, No. 6, 1969, pp. 1041–1059.

[16]Erdogan, F., and Gupta, G., "On the Numerical Solution of Singular Integral Equations," *Quarterly Journal of Applied Mathematics*, Vol. 23, 1972, pp. 525–534.

[17]Gladwell, G. M. L., *Contact Problems in the Classical Theory of Elasticity*, Sijthoff and Noordhoff, Alphen aan den Rijn, The Netherlands, 1980, pp. 209–212.

[18]Urquhart, E. E., "Frictionless Contact of Rigid Indenters on Multilayered Composite Half Planes," M.S. Thesis, Civil Engineering Dept., Univ. of Virginia, Charlottesville, VA, Feb. 1993.

[19]Shield, T. W., and Bogy, D. B., "Multiple Region Contact Solutions for a Flat Indenter on a Layered Elastic Half Space: Plane Strain Case," *Journal of Applied Mechanics*, Vol. 56, June 1988, pp. 251–262.

[20]Erdogan, F., "Fracture Mechanics of Functionally Graded Materials," *Composites Engineering*, Vol. 5, No. 7, 1995, pp. 753–770.

A. Palazotto
Associate Editor